

# **CATS Algorithm Theoretical Basis Document**

## **Level 1 and Level 2 Data Products**



### **Primary Authors:**

John E. Yorks, Science Systems and Applications, Inc., Lanham, MD, USA  
Stephen P. Palm, Science Systems and Applications, Inc., Lanham, MD, USA  
Matthew J. McGill, NASA Goddard Space Flight Center, Greenbelt, MD, USA  
Dennis L. Hlavka, Science Systems and Applications, Inc., Lanham, MD, USA  
William D. Hart, Science Systems and Applications, Inc., Lanham, MD, USA  
Patrick A. Selmer, Science Systems and Applications, Inc., Lanham, MD, USA  
Edward Nowotnick, GESTAR, Universities Space Research Asso., Columbia, MD USA

**Release 1.0**

12 June 2015

## Cloud-Aerosol Transport System

### CATS Algorithm Theoretical Basis Document

Prepared By:

---

John E. Yorks

Date

---

Stephen P. Palm

Date

---

Dennis L. Hlavka

Date

---

William D. Hart

Date

---

Patrick A. Selmer

Date

---

Edward Nowottnick

Date

Approved By:

---

Matthew J. McGill  
CATS Principal Investigator

Date

# Table of Contents

<b>1.0 Introduction .....</b>	<b>1</b>
<b>1.1 Purpose .....</b>	<b>1</b>
<b>1.2 Revision History .....</b>	<b>1</b>
<b>1.3 CATS Mission Overview .....</b>	<b>1</b>
<b>1.4 CATS Data Product Levels .....</b>	<b>3</b>
<b>2.0 Instrument Description.....</b>	<b>4</b>
<b>2.1 Transmitter Subsystems .....</b>	<b>4</b>
<b>2.2 Receiver Subsystems .....</b>	<b>5</b>
<b>2.3 Data Acquisition and Signal Processing.....</b>	<b>7</b>
<b>3.0 Overview of Level 1 Algorithms.....</b>	<b>8</b>
<b>3.1 Normalized Relative Backscatter .....</b>	<b>8</b>
<b>3.1.1 Geolocation of CATS Laser Beams.....</b>	<b>9</b>
<b>3.1.2 Detector Nonlinearity .....</b>	<b>11</b>
<b>3.1.3 Correction for Molecular Folding .....</b>	<b>12</b>
<b>3.2 Calibrated Backscatter.....</b>	<b>14</b>
<b>3.2.1 Ozone Transmission.....</b>	<b>14</b>
<b>3.2.2 Rayleigh Scattering .....</b>	<b>15</b>
<b>3.2.3 Polarization Gain Ratio .....</b>	<b>16</b>
<b>3.2.4 Stratospheric Scattering Ratios .....</b>	<b>21</b>
<b>3.2.5 Calibration at 532 and 1064 nm Wavelengths .....</b>	<b>23</b>
<b>3.2.6 Attenuated Backscatter .....</b>	<b>25</b>
<b>4.0 Overview of Vertical Feature Mask Algorithms .....</b>	<b>26</b>
<b>4.1 Atmospheric Layer Detection .....</b>	<b>26</b>
<b>4.2 Cloud-Aerosol Discrimination.....</b>	<b>26</b>
<b>4.3 Cloud Phase.....</b>	<b>26</b>
<b>4.4 Aerosol Typing.....</b>	<b>26</b>
<b>5.0 Overview of Geophysical Parameter Algorithms .....</b>	<b>27</b>
<b>5.1 Parameterized Lidar Ratio .....</b>	<b>27</b>
<b>5.2 Constrained Lidar Ratio .....</b>	<b>27</b>
<b>5.3 Modified Lidar Ratio .....</b>	<b>27</b>

## 1.0 Introduction

### 1.1 Purpose

This document describes the algorithms that will be used to calibrate the lidar backscatter profiles acquired by the CATS (Cloud-Aerosol Transport System) instrument flown aboard the International Space Station (ISS). The outputs of these algorithms are Level 1 data, consisting of attenuated backscatter coefficient profiles for the two channels (532 and 1064 nm) along with information on the uncertainties in these products. The Level 2 algorithms to produce geophysical parameters such as layer heights and optical depths use the Level 1 data. In addition, calibration files are generated that track the calibration constants that are derived during Level 1 processing. The data used by the Level 1 processing are geolocated prior to calibration.

### 1.2 Revision History

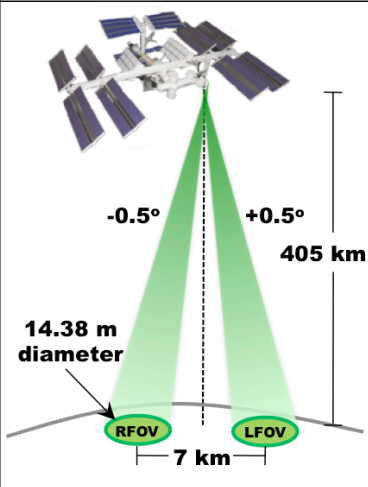
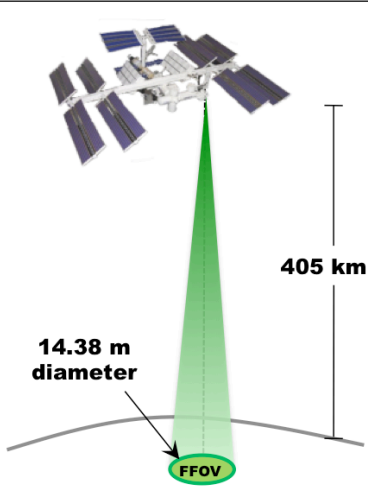
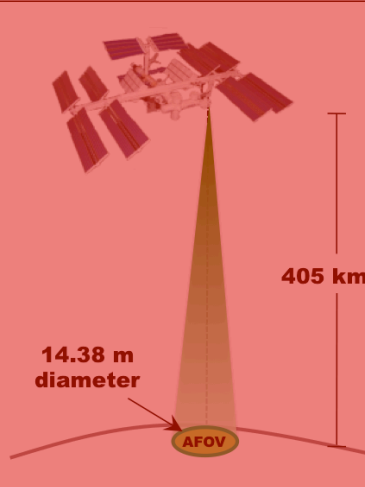
Issue Date	Release Number	Description	Lead Author	Sections Affected
06/12/15	1.0	Initial Release	John Yorks	1,2,3

### 1.3 CATS Mission Overview

The Cloud-Aerosol Transport System (CATS), launched on 10 January 2015, is a lidar remote sensing instrument that provides range-resolved profile measurements of atmospheric aerosols and clouds. Data from CATS is used to derive properties of cloud/aerosol layers including: layer height, layer thickness, backscatter, optical depth, extinction, and depolarization-based discrimination of particle type. The instrument is located on the Japanese Experiment Module – Exposed Facility (JEM-EF) on the International Space Station (ISS). The ISS orbit is a 51-degree inclination orbit at an altitude of about 405 km. This orbit provides more comprehensive coverage of the tropics and mid-latitudes than sun-synchronous orbiting sensors, with nearly a three-day repeat cycle. CATS is intended to operate on-orbit for at least six months, and up to three years. The CATS payload is designed to provide a combination of long-term operational science, in-space technology demonstration, and technology risk reduction for future Earth Science missions.

The measurements of atmospheric clouds and aerosols provided by the CATS payload are used for three main science objectives. 1) One important aspect of the CATS on-orbit science is to provide real-time observations of aerosol vertical distribution as inputs to global models. The vertical profile information obtained by CATS, particularly at multiple wavelengths and with depolarization information obtained in Mode 1 and 2,

provides height location of cloud and aerosol layers, as well as information on particle size and shape. 2) Another important aspect of the CATS on-orbit science is to extend the space-based lidar record for continuity in the lidar climate observations. The CATS instrument provides measurements of cloud and aerosol profiles similar to CALIPSO, filling in the data gap, so this information can continually be used to improve climate models and our understanding of the Earth system and climate feedback processes. 3) Finally, CATS advances technology in support of future space-based lidar mission development by demonstrating the ability to retrieve vertical profiles using a high repeat-rate laser and photon counting detection, as well as the testing of component for the High Spectral Resolution Lidar (HSRL) technique and 355 nm wavelength.

<b>Mode 7.1: Multi-Beam</b>	<b>Mode 7.2: HSRL Demo</b>	<b>Mode 7.3: UV Demo</b>
Backscatter: 532, 1064 nm No HSRL Depolarization: 532, 1064 nm	Backscatter: 532, 1064 nm HSRL: 532 nm Depolarization: 1064 nm	Backscatter: 355, 532, 1064 nm No HSRL Depolarization: 532, 1064 nm
		
Semi-continuous operation: Feb. 10 – Mar. 21 Failure: under investigation	Semi-continuous operation: Mar. 25 – Present Future Mode of Operation	Failure in laser optics No data available

**Figure 1.1** CATS three main Science Modes for operation, with details of each mode’s capabilities and operational status.

To meet these three science goals, CATS operates in three different modes using four instantaneous fields of view (IFOV) as shown in Figure 1.1:

- **Mode 7.1: Multi-beam backscatter detection at 1064 and 532 nm, with depolarization measurement at both wavelengths.** The laser output is split into two transmit beams, one aimed 0.5° to the left and one 0.5° to the right, effectively making two tracks separated by 7 km (~4.3 mi) at Earth’s surface. This operational mode will be used to ensure that minimum science requirements can be met for the maximum mission duration.

- **Mode 7.2: Demonstration of HSRL aerosol measurements.** This mode uses the injection-seeded laser operating at 1064 and 532 nm to demonstrate a high spectral resolution measurement using the 532-nm wavelength.
- **Mode 7.3: Demonstration of 355-nm profiling.** This mode uses the injection-seeded laser operating at 1064, 532, and 355 nm to demonstrate 355-nm laser performance. Similar to the backscatter detection mode, there are depolarization measurements at each wavelength

## 1.4 CATS Data Product Levels

The CATS Level 1B and 2 data processing algorithms rely heavily on heritage from existing airborne and space-based lidar systems, such as the Cloud Physics Lidar (CPL, McGill *et al.* 2002), the Airborne Cloud-Aerosol Transport System (ACATS, Yorks *et al.* 2014), and the Cloud-Aerosol Lidar Infrared Pathfinder Spaceborne Observations (CALIPSO) satellite (Winker *et al.* 2009). The HSRL data processing algorithms will be very similar to those used for the ACATS instrument, with much longer turnaround times expected.

The data products generated from the ATS measurements are produced according to a protocol that is similar to that established by NASA's Earth Observing System (EOS), but are not required to meet any specific protocol. The CATS data product levels are defined as follows:

- **Level 0:** reconstructed, unprocessed instrument data at raw resolutions (i.e., the downlinked raw photon counts from the CATS instrument). Any and all communications artifacts (e.g. synchronization of packets, communications headers, duplicate or missing data) are removed in the L0 process.
- **Level 1A:** Level 0 data that is time-referenced, geo-located, corrected for detector nonlinearity and instrument artifacts, normalized to laser energy, and annotated with ancillary information. The CATS Level 1A data (relative normalized backscatter) is an internal product only and is not distributed.
- **Level 1B:** Level 1A data that have been calibrated, annotated with ancillary meteorological data, and processed to sensor units. The CATS Level 1B data (attenuated total backscatter and depolarization ratio) is archived as Level 1 data.
- **Level 2:** Geophysical parameters derived from Level 1 data, such as the vertical feature mask, profiles of cloud and aerosol properties (i.e. extinction, particle backscatter), and layer-integrated parameters (i.e. lidar ratio, optical depth). There will be two CATS Level 2 products:
  - **CATS Heritage L2:** L1B files that are run through the CALIPSO L2 algorithms to provide continuity in the algorithms used for the lidar climate record.
  - **CATS Operational L2:** L1B files that are run through the new operational CATS L2 algorithms, which will include new capabilities that correspond to new instrument technology.

## 2.0 Instrument Description

The CATS payload is based on existing instrumentation built and operated on the high-altitude NASA ER-2 aircraft. The instrument consists of 2 high repetition rate Nd:YVO<sub>4</sub> lasers operating at three wavelengths (1064, 532, and 355 nm) that generate signal photons, a receiver subsystem with a 60 cm diameter telescope to collect photons that backscatter from the atmosphere, and a data system to provide timing of the return photon events. The CATS instrument parameters are given in more detail in Table 2.1.

### 2.1 Transmitter Subsystems

The CATS laser transmitter that will be used in Mode 7.1, referred to as Laser 1, gets its heritage from the Cloud Physics Lidar (CPL; McGill *et al.* 2002) instrument. It is a Nd:YVO<sub>4</sub> laser with a repetition rate of 5000 Hz and an output energy of about 1 mJ per pulse at 532 and 1064 nm. An image of the laser 1 bench assembly is shown in Figure 2.1.

**Table 2.1. CATS Instrument Parameters.**

<b>Laser 1 Type</b>	<b>Nd: YVO<sub>4</sub></b>
<b>Laser 1 Wavelengths</b>	<b>532, 1064 nm</b>
<b>Laser 1 Rep. Rate</b>	<b>5000 Hz</b>
<b>Laser 1 Output Energy</b>	<b>~1 mJ/pulse</b>
<b>Laser 2 Type</b>	<b>Nd: YVO<sub>4</sub>, seeded</b>
<b>Laser 2 Wavelengths</b>	<b>355, 532, 1064 nm</b>
<b>Laser 2 Rep. Rate</b>	<b>4000 Hz</b>
<b>Laser 2 Output Energy</b>	<b>~2 mJ/pulse</b>
<b>Telescope Diameter</b>	<b>60 cm</b>
<b>View Angle</b>	<b>0.5 degrees</b>
<b>Telescope FOV</b>	<b>110 microradians</b>

The frequency characteristics of pulsed lasers have recently been advanced due to the development of direct detection Doppler lidars and HSRLs. These techniques impose further requirements compared to standard backscatter lidars, such as lasers that are single frequency on a single pulse basis and more stable in time (central frequency drift of less than 1 MHz per minute). An injection-seeded, pulsed Nd: YVO<sub>4</sub> laser was developed for CATS, with heritage from a similar laser transmitter built for the Airborne Cloud-Aerosol Transport System (ACATS: Yorks *et al.* 2014), that achieves these frequency characteristics (Hovis *et al.* 2004). This laser, referred to as Laser 2 and shown in Figure 2.2, provides a narrow wavelength distribution suitable for resolving the small frequency shifts due to the Doppler effect. The laser operates at an output power of about 2 mJ per pulse and repetition rate of 4000 Hz. This seeded laser also contains an external frequency-tripling module to provide output at 355 nm for Mode 7.3 that should failure occur, will not negatively impact operations at 532 and 1064 nm.

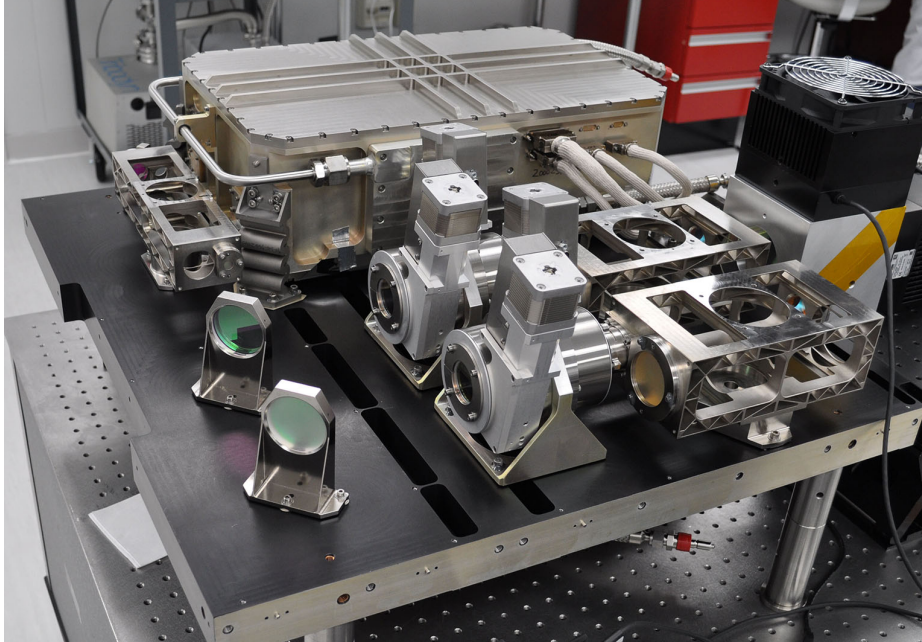


**Figure 2.1** The CATS laser 1 bench assembly for 532 and 1064 nm operation.

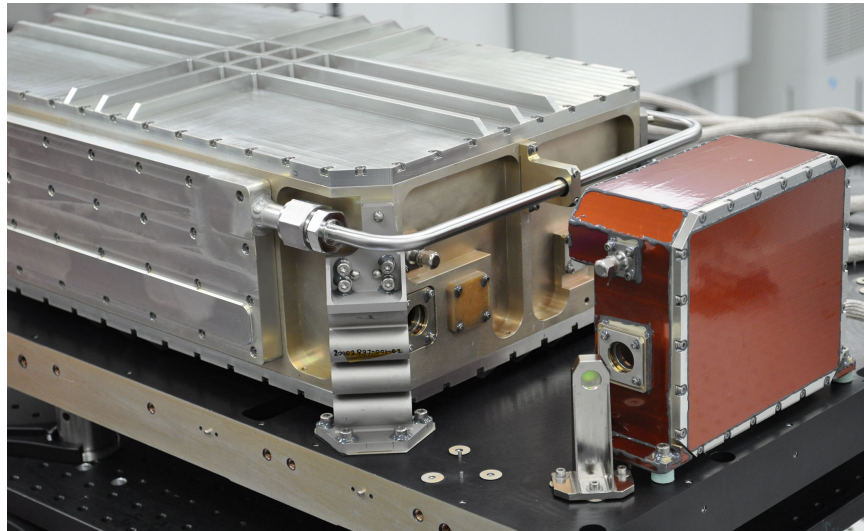


**Figure 2.2** The CATS laser 2 bench assembly with the external frequency-tripling module (orange).

## 2.2 Receiver Subsystems

CATS employs a 60 cm beryllium telescope that has a 110 microradian field of view, allowing for a 0.5 degree view angle. The telescope, shown in Figure 2.3, is also fiber-coupled to the detector boxes to provide greatest flexibility. CATS contains four detector boxes. Beam splitters are used to measure the parallel and perpendicular polarized return in all four detector boxes. The first two detector boxes are identical and are used for the



LFOV and RFOV of Mode 7.1. Each of these detector boxes contain six detector channels for the following detection:

- 532 nm Parallel Backscatter (2)
- 532 nm Perpendicular Backscatter (2)
- 1064 nm Parallel Backscatter
- 1064 nm Perpendicular Backscatter

A third and similar detector box is used for Mode 7.3 that contains the same 6 channels as the Mode 7.1 detector boxes, plus 1 additional 355 nm Total Backscatter channel for a total of 7 channels. These three detector boxes are shown in Figure 2.4. The final detector box, referred to as the HSRL detector box, contains 12 detector channels: 10 designated as 532 nm HSRL channels, one 1064 nm Parallel and one 1064 nm Perpendicular backscatter channel.

The heart of the CATS HSRL detector box is an etalon that provides the spectral resolution needed for the HSRL measurement. Backscattered light collected by the telescope is passed through the etalon and an image of the etalon fringe pattern is created. A bandpass filter is used in tandem with the etalon to reject background sunlight, permitting daytime operation. The optical gap of the etalon is 3 cm with a plate reflectivity of 90%. It is critical to maintain the symmetry and shape of the etalon fringe pattern to avoid uncertainty in the measurement. A digital etalon controller was developed by Michigan Aerospace Corporation in which piezoelectric actuators control the etalon electronics to position and maintain the plate parallelism. A holographic circle-to-point converter optic (McGill *et al.* 1997c; McGill and Rallison 2001) is placed in the focal plane of the HSRL receiver to provide the spectral detection. The circle-to-point converter simplifies hardware requirements, improves efficiency of measuring the spectral content in the fringe pattern, and allows CATS to utilize photon-counting detection. The holographic optic is coupled to the 10 individual 532 nm detectors, each representing a small wavelength interval.



**Figure 2.3** The CATS 60 cm beryllium telescope prior to full instrument assembly.



**Figure 2.4** The three standard backscatter detector boxes for Modes 7.1 (LSFOV and RSFOV) and 7.3.

## 2.3 Data Acquisition and Signal Processing

During Level 0 processing, data are time-sorted and corrected for communication artifacts (i.e. duplicate or missing data). Raw CATS data, with 60 m (Mode 7.1; 78 m for Mode 7.2) vertical resolution and 350 m horizontal resolution, are received from the ISS in real-time during acquisition-of-signal (AOS) periods. During loss-of-signal (LOS) periods, which can range from 1 minute to 2 hours, data are not received real-time. CATS

data are recorded on-board the ISS during LOS periods then transmitted to the ground during subsequent AOS periods. Due to the LOS periods, data are collected at the CATS ground station in 3-hour segments to ensure all data can be sorted properly. Level 0 files are created once two 3-hour segments have been obtained. Every time a new segment is collected, the previous segment is processed into Level 0 files using the new segment to fill in data gaps caused by LOS periods. Thus, Level 0 files are produced every 6 hours. The ISS time data, which is reported in the CATS Level 0 files, is corrected for drift using a special ISS data stream during Level 0 processing.

Level 0 files are partitioned into either day or night “granule” files based on two criteria. These criteria are:

- 1) The z-component of the solar line-of-sight unit vector reported in the ISS Broadcast Ancillary Data (BAD) must meet a threshold value of greater than 0.0 in order for a file to be deemed night. A value less than 0.0 would be classified as day.
- 2) The solar background counts for the given profile must cross a threshold value of 6 counts to be classified as day. A profile is classified as night if the solar background counts are less than 6.

A new granule file is produced when both criteria agree for a given profile and these granules are then labeled correspondingly as either a “day” file or “night” file. It should be noted that there are occasions when the 6-hour sorting window is not large enough to fill in the data gaps caused by out-of-sequence data. In this scenario, two granules may be produced, with 4.5 minutes between the start and end times of the granules, instead of one larger granule.

## **3.0 Overview of Level 1 Algorithms**

### **3.1 Normalized Relative Backscatter**

The CATS Level 1A data is referred to as the Normalized Relative Backscatter (NRB) and is an internal product only that is not distributed. The NRB data is Level 0 data that is geolocated, corrected for detector nonlinearity and the folding of molecular signal from the atmosphere above, normalized to laser energy, and annotated with ancillary information. The ancillary information included in the NRB data is the Broadcast Ancillary Data (BAD) from the ISS that describes the environment in which a payload is operating. The BAD is sent at a rate of 10 Hz and includes the roll, pitch and yaw of the ISS, the quaternion, and the CTRS position information. Since the CATS laser points off-nadir 0.5 degrees in any of the three science modes, and has multiple beams in Mode 7.1, the geolocation of the CATS laser beam is computed for each FOV using the BAD and the CATS relative angles. More information on the algorithm to determine the geolocation of each CATS FOV is provided in section 3.1.1. Once the data is geolocated, the raw photon counts are corrected for detector nonlinearity (D), as described in

section 3.1.2. The Normalized Relative Backscatter ( $\beta'_{NR}$ ) for each wavelength and range bin is then computed using the equation:

$$\beta'_{NR}(r) = \frac{\{[N(r) * D] - N_B\}r^2}{E} \quad \text{Eq. 3.1}$$

where  $r$  is the range at each range bin and  $E$  is the laser energy as measured by energy monitors installed on the CATS instrument. The solar background photon counts ( $N_B$ ) is estimated by averaging the signal below the earth's surface. All the products reported in the CATS L1A data products are used as input to the CATS L1B data products.

### 3.1.1 Geolocation of CATS Laser Beams

Knowledge of the location of the CATS laser spot on the earth is required for the useful analysis of the CATS backscatter data. The location of the CATS laser spots can be calculated from the position, velocity, and attitude information found in the ISS Broadcast Ancillary Data (BAD) together with the known angular offset of the laser line-of-site (LOS) vector from the instrument's nadir vector. The computation requires a series of coordinate transformations and rotations to find the geodetic latitude and longitude of the laser spot at the height of the Digital Elevation Model (DEM).

The CATS algorithm uses four coordinate systems in the computation of the laser spot location, which include:

- 1) The CATS instrument body (LOS) reference frame
- 2) The local vertical local horizontal (LVLH) reference frame
- 3) The Conventional Terrestrial or geocentric (CTRS, x,y,z) reference frame
- 4) The geodetic reference frame (longitude, latitude, altitude).

Because angular offsets between the ISS body reference system and the CATS body reference system are unknown, the two systems are considered to be the same. The difference is assumed to be small so the BAD data that is referenced to the ISS body is considered to be reference to the CATS body.

The ISS body position data ( $x_{iss}, y_{iss}, z_{iss}$ ) and velocity data ( $v_{xiss}, v_{yiss}, v_{ziss}$ ) are contained in the ISS BAD. These vectors can be used to construct the LVLH unit vector  $\vec{M}_{vh}$ , along with the following information.

- 1) The forward velocity unit vector of the ISS
- 2) The nadir unit vector
- 3) The cross product of the forward velocity unit vector of the ISS and the nadir unit vector for a right handed coordinate system
- 4) The geocentric unit vector of the ISS
- 5) The speed and distance from the earth's center, respectively

The ISS attitude data is also included in the BAD in the form of quaternion components ( $q_{wiss}, q_{xiss}, q_{yiss}, q_{ziss}$ ), which are the scalar and x, y, z vector quaternion components referenced to the LVLH reference frame. These quaternion components can be converted to the yaw, pitch, and roll ( $a_y, a_p, a_r$ ). Yaw, pitch, and roll can be used to construct a matrix to transform the laser LOS vector into the LVLH reference system. The matrix is:

$$M_{ypr} = \begin{pmatrix} C_y C_p & -S_y C_r - C_y S_p S_r & S_y S_r \\ S_y C_p & C_y C_r - S_y S_p S_r & -C_y S_r - S_y S_p C_r \\ S_p & C_p S_r & C_p C_r \end{pmatrix} \quad \text{Eq. 3.2}$$

where C and S represent functions cosine and sine and subscripts y, p, and r refer to yaw, pitch, and roll, respectively. By using the LVLH unit vector and equation 3.2, the CATS laser pulse location at a sampling bin in geodetic coordinates can be found using the following steps.

- 1) Compute geodetic coordinates of ISS ( $a_{tgd} \ a_{ngd} \ h_{gd}$ )= $V(x_{iss}, y_{iss}, z_{iss})$ , where ( $a_{tgd} \ a_{ngd} \ h_{gd}$ )= geodetic latitude, longitude, and altitude of the ISS and  $V(x,y,z)$  is the Vermeille transformation from geocentric to geodetic coordinates (Vermeille 2002).
- 2) Define the LOS vector for the appropriate CATS laser pointing direction, fore, aft, left, or right. The CATS body reference system is defined by positive x-axis along the forward direction, positive y-axis to the left, and positive z-axis toward the earth. A LOS vector is defined in spherical coordinates by the rotation about the z-axis ( $\phi$ ), angle from the x-y plane ( $\theta$ ) and range from CATS ( $R_B$ ). For all four pointing directions,  $\theta=(\pi/2 - 0.008)$  radians. For fore, aft, left, and right  $\phi=0, \pi, \pi/2$ , and  $3\pi/2$ , respectively. So, in Cartesian coordinates, the laser LOS vector is:

$$(x_{Bis} \ y_{Bis} \ z_{Bis}) = (R_B \cos \phi \cos \theta \ R_B \sin \phi \cos \theta \ R_B \sin \theta) \quad \text{Eq. 3.3}$$

- 3) Use  $M_{ypr}$  from equation 3.2 to transform the laser LOS vector to LVLH reference frame.
- 4) Use the LVLH unit vector ( $M_{vh}$ ) to convert ( $x_{Bvh} \ y_{Bvh} \ z_{Bvh}$ ) to the geocentric reference frame. This conversion results from the following equations.
- 5) Compute the geocentric coordinates of the laser spot by adding Cartesian coordinates in the geocentric reference to the ISS coordinates.
- 6) Convert the laser spot coordinates to geodetic reference frame by using Vermeille's transformation.
- 7) Compute the CATS laser LOS vector in the geodetic reference frame for a series of range bins  $R_{bi}$  that will positively pass through the altitude of the local DEM. Select the location where z-component of the CATS laser LOS vector most closely matches the altitude reported by the DEM. The latitude and longitude of that bin will be the latitude and longitude of the laser spot.

The DEM values used are average values for 1 km by 1km grid boxes. This will lead to some discrepancies in the latitude and longitude of the CATS laser spot in mountainous terrain.

### 3.1.2 Detector Nonlinearity

The measured CATS signal can become erroneously low when measuring targets that strongly backscatter light due to detector dead time and must be compensated for. All lidar systems that employ photon-counting detection experience this effect, which is a limitation on the number of photons that can be counted in a given time interval. For CATS, highly reflective features, such as bright surfaces (desert, sea ice) and water clouds push the detector into a nonlinear counting region. A typical photon counting detector, such as the ones employed in CATS, has a discriminator dead time of 28 to 30 ns for a discriminator maximum count rate on the order of 30 MHz.

The nonlinear effects for this type of detector can be quantified by a detector dead time coefficient. This coefficient represents the fact that only one photon event can be counted at once, and the detector system has a certain time delta, or dead time, before it can count another. If the mean time between events is much greater than the dead time, then it can be shown that

$$N_{a,i} = \frac{N_{m,i}}{1 - \left( \frac{N_{m,i} \tau}{\Delta t} \right)} \quad \text{Eq. 3.4}$$

where  $N_{m,i}$  is the measured counts on channel  $i$ ,  $N_{a,i}$  is the counts that would be sensed if the detector were completely linear,  $\Delta t$  is the total integration time, and  $\tau$  is the dead time. These nonlinear effects can be significantly reduced by applying Eq. 3.4 to the measured signal, which allows for a reasonable correction of the atmospheric data bins. The CATS detectors rarely experience count rates higher than 35 MHz in atmospheric bins below 28 km. Therefore, the detector dead time coefficient is less than 1.10 for 99.0% of atmospheric bins. An example of the CATS deadtime correction factors, as a function of photon counts, are shown in Figure 3.1 for detector 1 (RFOV 1064 nm parallel channel).

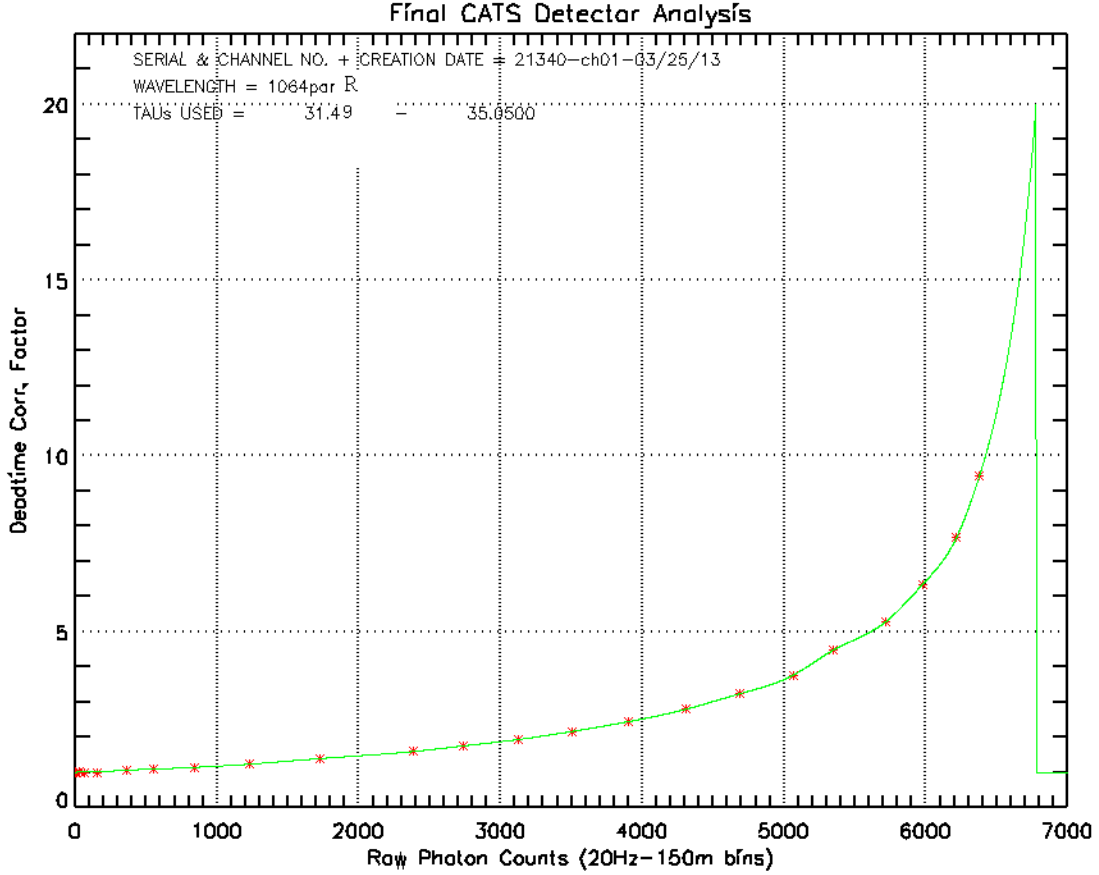


**Figure 3.1** The CATS deadtime correction factors for RFOV 1064 nm parallel channel detector as a function of photon counts.

### 3.1.3 Correction for Molecular Folding

The raw photon data captured by CATS at range  $r$  (where  $r < 28$  km) will have contributions from atmospheric scattering at heights  $z+Nx$  km, where  $N=1,2,3$ , etc. and  $x = 30$  for operating mode 7.1 and 37.5 for mode 7.2. This effect is caused by the high repetition rate of the CATS lasers discussed in section 2.2. In practice, only  $N=1$  is important as scattering above 60 km is negligible. The folding of molecular scattering is important to remove because accurate background cannot be calculated without doing so. Background is computed from the 2 km of data below the ground. However, the data in this region contains molecular scattering from the 28 to 30 km region of the atmosphere. If this signal is not removed, it becomes part of the calculated background. If this background is subtracted from each bin of the profile, it will remove most of the photon counts from true molecular scattering in the calibration zone (23-27 km altitude). This will render accurate calibration from the molecular signal impossible.

The molecular contribution to the measured photon count can be computed from equation 3.3:

$$N_m(r, \lambda) = \frac{N_e(\lambda)}{r^2} \beta_m(r, \lambda) \Delta r A_t T_m^2(r, \lambda) T_o^2(r) Q_e T_{opt} N_a R(r, \lambda) \alpha(\lambda) \quad \text{Eq. 3.5}$$

Where  $N_e$  is the number of photons transmitted by CATS which is defined by the laser energy ( $E$ ) as:

$$N_e = \frac{E(\lambda)\lambda}{hc} \quad \text{Eq. 3.6}$$

Where  $\lambda$  is the laser wavelength (532 nm),  $h$  is the Planck constant and  $c$  is the speed of light. The other terms used in equation 3.5 above are:

- $r$  – The range from the satellite to the height  $z$  (in m).
- $\beta_m(r)$  – the molecular backscatter cross section at range  $r$  ( $\text{m}^{-1} \text{sr}^{-1}$ ).
- $\Delta r$  – the bin size in meters (60 m)
- $A_t$  – Area of telescope (m, effective)
- $T_m(r)$  – Molecular atmospheric transmission from top of atmosphere to range  $r$ .
- $T_o(r)$  – Ozone transmission: top of atmosphere to range  $r$ .
- $Q_e$  – Quantum efficiency of detector
- $T_{opt}$  – Transmission of the receiver system optics
- $N_a$  – Number of shots summed (nominally 250)
- $R(r)$  – aerosol scattering ratio
- $\alpha(\lambda)$  - scaling factor

In equation 3.5,  $\alpha$  is used to adjust the computed photon count since the exact values of quantities like system optical transmission ( $T_{opt}$ ) and detector quantum efficiency ( $Q_e$ ) are not known exactly and moreover, can change with time. The value of  $\alpha$  was computed empirically by adjusting it until the slope of the average NRB signal (for a granule) above 20 km matched the slope of the average modeled molecular backscatter, which is derived using the technique described in section 3.2.2. It was found that too low of an alpha will produce a slope less than the molecular model, and a value too large will produce too large a slope. Further, it was found that alpha varies only slowly with time and requires only infrequent tuning. Alpha is computed empirically for each wavelength and each field of view. Typical values of alpha range from 0.04 to 0.08 for the 1064 nm channel and 0.02 to 0.07 for the 532 nm channel.

Equation 3.5 is used to compute a profile of molecular scattering contribution from 58 km to 28 km ( $N_m(r)$ ). From that profile, the molecular scattering contribution (folded from above) to the measured CATS photon profile is computed as:

$$N'_m(r) = N_m(r + x) \quad \text{Eq. 3.7}$$

Where  $x = 30$  km for operating mode 7.1 and  $x = 37.5$  for operating mode 7.2. For  $r$  between -2 and 28 km. Then the corrected raw photon count profile is:

$$S'(r) = S(r) - N'_m(r) \quad \text{Eq. 3.8}$$

Where  $S(r)$  is the raw photon count profile measured by CATS. Note that this process leaves the molecular scattering of the original profile ( $S(r)$ ) intact. It only removes the



molecular scattering folded down from above. The NRB corrected for the molecular folding can now be computed as:

$$NRB'(r) = (S'(r) - N_B)/E = C\beta(r)T^2(r) \quad \text{Eq. 3.9}$$

### 3.2 Calibrated Backscatter

The processing algorithms for Level 1B in Modes 1 and 3 consist mainly of the backscatter and depolarization calibrations. The 532 nm CATS data is calibrated by normalizing the NRB signal to the 532 nm molecular backscatter signal in a set calibration region (Russell *et al.* 1979, Del Guasta 1998, McGill *et al.* 2007, Powell *et al.* 2009). The CATS calibration region is 23-27 km, starting 1 km below the top of the CATS data frame (28 km). The aerosol loading in this region is computed using CALIPSO data and applied to the calibration. The CATS NRB signal is averaged to 4 minutes at night and 46 minutes during daytime operation to reduce uncertainty in the calculation. During nighttime data collection, the 1064 nm calibration constant can be computed using an identical approach as the 532 nm calculation. However during daytime operation, the 532 and 1064 nm signal is often calibrated using a default value derived from historical data or manual normalization to the Rayleigh backscatter model. The polarization gain ratio, which describes the relative gain between polarization channels, is computed for both 532 and 1064 using the solar radiation scattered by ice clouds (Liu *et al.* 2004).

#### 3.2.1 Ozone Transmission

The ozone transmission,  $T_o^2(r)$ , is calculated using ozone mass mixing ratios obtained from the GMAO meteorological data set, which contains ozone mass mixing ratios. The ozone mass mixing ratios,  $r_o(r)$  are first converted to column density per kilometer (atm-cm/km),  $\epsilon_o(r)$ , using the following equation:

$$\epsilon_o(r) = \frac{r_o(r)\rho(r)}{2.14148 \times 10^{-5}} \quad \text{Eq. 3.10}$$

where  $r$  is the range in km, and  $\rho(r)$  is the atmospheric density at  $r$  and calculated from the meteorological data as:

$$\rho(r) = \frac{P(r)}{RT(r)} \quad \text{Eq. 3.11}$$

The next step is to calculate the ozone transmission term,  $T_o^2(\lambda)$ , which is computed using the following equation:

$$T_o^2(\lambda, r) = \exp\left[-2c_o(\lambda) \int_H^r \epsilon_o(r') dr'\right] \quad \text{Eq. 3.12}$$

where  $c_o(\lambda)$  is the Chappius ozone absorption coefficient in  $\text{cm}^{-1}$  and  $\lambda$  is 532 nm. The ozone absorption coefficient is obtained at the correct wavelength from a table compiled in Iqbal (1984) using data from Vigroux (1953). The 532 nm Chappius ozone absorption coefficient used is  $0.065 \text{ cm}^{-1}$ . The 1064 nm coefficient is  $\sim 0.0 \text{ cm}^{-1}$ .  $H$  is nominally 60 km.

The ozone transmission is then modified to account for the off-nadir angle of the CATS laser beam. The off-nadir angle varies by CATS FOV and its computation is detailed in section 3.1.1. If  $\theta$  is the off-nadir angle of the laser beam, the angle correction to the transmission is:

$$T_o^2(\lambda, r) = T_o^2(\lambda, r)^{\sec(\theta)} \quad \text{Eq. 3.13}$$

The application of the ozone transmission to the CATS calibration method is described in section 3.2.5.

### 3.2.2 Rayleigh Scattering

This section provides a brief introduction to atmospheric molecular scattering as it relates to CATS and describes the molecular scattering parameters computed for use in CATS data processing. Atmospheric molecular scattering consists of two components. Rayleigh scattering is considered elastic scattering from particles that are very small compared to the wavelength of the scattered radiation, such as molecules. Vibrational Raman scattering has a scattering cross section that is very small compared to Rayleigh scattering, so it is neglected when computing the molecular scattering (Bucholtz 1995; Bodhaine *et al.* 1999; She 2001). For lidar applications, the phrases Rayleigh scattering and molecular scattering are used as synonyms. The main sources of Rayleigh-scattered light are nitrogen and oxygen, since these two gases accounts for about 99% of the Earth's molecular atmosphere. The Rayleigh scattering intensity is related to the wavelength of incident radiation ( $\lambda$ ) through the relationship  $\lambda^{-4}$  and dominates backscatter signals from elastic backscatter lidars at short laser wavelengths. For elastic backscatter lidars such as CATS, the Rayleigh scattering signal is used to normalize the total return signal and determine the instrument calibration constant. Additionally, the molecular backscatter coefficient ( $\beta_M$ ) and molecular extinction coefficient ( $\sigma_M$ ) must be known to reduce the unknown parameters in the standard lidar equation to two.

The molecular backscatter coefficient is determined from Rayleigh scattering theory (Tenti *et al.* 1974; Young 1981) and is proportional to atmospheric density. Thus, the molecular backscatter coefficient can be computed using its relationship to atmospheric temperature and pressure, as demonstrated by Collis and Russell (1976), through the equation:

$$\beta_M = \frac{P}{KT} (5.45 \times 10^{-32}) \left( \frac{\lambda}{550} \right)^{-4.09} \quad \text{Eq. 3.14}$$

where  $T$  is the atmospheric temperature in units of Kelvin,  $p$  is the atmospheric pressure in units of hPa and  $K$  is the Boltzmann constant ( $1.38 \times 10^{-23} \text{ J K}^{-1}$ ). Furthermore, the molecular extinction coefficient ( $\sigma_M$ ) is resolved from the molecular backscatter coefficient through the relationship:

$$\sigma_M = \beta_M \left( \frac{8}{3} \right) \pi \quad \text{Eq. 3.15}$$

The NASA Global Modeling and Assimilation Office (GMAO) provide a forecast of the atmospheric temperature and pressure profiles for 72 vertical levels (0-60 km AMSL) at a horizontal resolution of 10 seconds that is subset along the ISS orbit track. The temperature and pressure from GMAO are interpolated to the CATS vertical bin width of 60 m over a range of 0 to 60 km AMSL to better match the vertical structure of the CATS lidar backscatter data. The molecular backscatter and extinction coefficients are computed using equations 3.14 and 3.15, respectively. These parameters, along with the interpolated temperature, pressure, and other GMAO variables are output in the Level 1B files. Errors in the forecasted GMAO are estimated to be 0.5 K for profiles of temperature (Prive' *et al.* 2012) and 1 hPa for surface pressure (Reinecker *et al.* 2008).

In cases when the parallel-polarized backscatter channel is normalized to the attenuated molecular backscatter, the molecular depolarization ratio ( $\delta_M$ ) must be considered. The depolarization ratio is defined and the ratio of perpendicular to parallel backscatter. The molecular depolarization ratio for the three CATS wavelengths is given in Table 3.1, as provided by the CALIPSO ATBD and Behrendt and Nakamura (2002). These values are used to compute an attenuated molecular backscatter for the parallel-polarized light and reduce error in the CATS calibration constant when normalizing the parallel channel to Rayleigh backscatter.

**Table 3.1.** CATS molecular depolarization ratios for three operating wavelengths

$\lambda$ (nm)	$\delta_m$ (%)
355	1.554
532	1.430
1064	1.400

### 3.2.3 Polarization Gain Ratio

Pulsed lasers, such as the ones used in the CATS instrument, naturally produce linearly polarized light. Using a beam splitter in the receiver optics, the perpendicular and parallel planes of polarization of the backscattered light are measured. The linear volume depolarization ratio is defined as the ratio of perpendicular total (Rayleigh plus particle) backscatter to parallel total backscatter, and has values between 0.2 and 0.6 for non-spherical particles such as ice crystals (Sassen and Benson 2001; Yorks *et al.* 2011a). Deriving accurate depolarization ratios from CATS data requires knowledge of the relative gain between the perpendicular and parallel channels of the CATS receiver,

referred to as the polarization gain ratio (PGR).

The CATS operational PGR consists of two terms. The equation for the CATS operational PGR is:

$$PGR_{OP} = PGR_1 \times PGR_2 \quad \text{Eq. 3.16}$$

The first term,  $PGR_1$ , characterizes the relative gain between the perpendicular and parallel channels at both the 532 and 1064 nm wavelengths. The second term,  $PGR_2$ , corrects for poor depolarization purity in the 532 nm measurements.

The algorithm to compute  $PGR_1$  uses the ratio of the parallel to perpendicular solar background radiation scattered from dense ice clouds, as outlined by Liu *et al.* (2004). The background light measured by CATS is the scattering of solar radiation by the surface, clouds, aerosols, and molecules in the atmosphere. The difference in solar background counts between the parallel and perpendicular channels is minimal since the solar radiation scattered by dense ice clouds is unpolarized in theory (Liou *et al.* 2000). Dense ice clouds used to compute the first polarization gain ratio term during daytime periods only include only the top cloud layers and are identified using four criteria:

- 1) **Mid-cloud temperature ( $T_M$ ):  $T_M < -35$  C**
- 2) **532 nm (mode 7.1) or 1064 nm (mode 7.2) integrated attenuated total backscatter ( $\gamma_{1064}$ ):  $0.008 < \gamma_{1064} < 0.044$  sr<sup>-1</sup>**

where:

$$\gamma_{1064} = \int_{bottom}^{top} \beta_{1064} T_{1064}^2 dz \quad \text{Eq. 3.17}$$

- 3) **1064 nm layer-integrated depolarization ratio ( $\delta_{\lambda\alpha\psi}$ ):  $0.30 < \delta_{\lambda\alpha\psi} < 0.80$**

where:

$$\delta_{1064} = \frac{\sum_{layer} NRB_{perp}}{\sum_{layer} NRB_{par}} \quad \text{Eq. 3.18}$$

- 4) **532 nm (mode 7.1) or 1064 nm (mode 7.2) optical depth ( $\tau_{1064}$ ):  $\tau_{1064} > 1.75$**

This criteria is actually assessed using the two-way transmission ( $T_C^2$ ) of the threshold optical depth, which is computed using the equation

$$T_C^2 = e^{-2\tau_c} \quad \text{Eq. 3.19}$$

and compared to the two-way transmission of the layer ( $T_{lay}^2$ ) as estimated below:

$$T_{lay}^2 = 1 - S \times \gamma_{1064} \quad \text{Eq. 3.20}$$

where S is the lidar ratio estimated as 25 sr for dense ice clouds.

The polarization gain ratio can then be derived using the ratios of the parallel and perpendicular background signals summed over the entire granule from all profiles within the granule file that contain these “dense ice clouds”. Using a similar procedure, Liu *et al.*

(2004) found polarization gain ratios for CALIPSO data that compared favorably with the values measured onboard by inserting a half-wave plate with its optical axis aligned at 22.5 degrees to the transmitted laser polarization direction into the optical path of the transmitter (Spinhirne *et al.* 1982) or the receiver (McGill *et al.* 2002).

The CATS depolarization purity at 1064 nm was measured in the lab at GSFC as greater than 200:1 before launch. However, the depolarization purity at 532 nm was measured at about 7:1. To improve the accuracy of CATS 532 nm depolarization measurements, this data must be corrected for this poor depolarization purity at 532 nm. A separate measurement of depolarization ratio is necessary to compare to the CATS measurements at both 1064 and 532 nm and estimate the  $PGR_2$  term. The Cloud Physics Lidar (CPL; McGill *et al.* 2002) is an airborne elastic backscatter lidar system that flies aboard the NASA ER-2 high altitude aircraft and operates at 1064, 532, and 355 nm wavelengths. Depolarization is resolved using the 1064 nm channel and cloud optical properties are retrieved using the 1064 and 532 nm channels (McGill *et al.* 2003). CPL flew aboard the ER-2 during the month of February 2015 out of Palmdale, CA. During this time, the ER-2 flew under the ISS track on four occasions. One such flight on 22 February occurred during local nighttime hours and included observations of dense ice clouds along the ISS track. Figure 3.2 shows the ISS track in black, nearly parallel to the California coastline and the ER-2 track in red, both of which intercept ice clouds (light tan and blue colors). The ER-2 flew about a 30-minute segment below the ISS in which CPL and CATS collected near-coincident data.

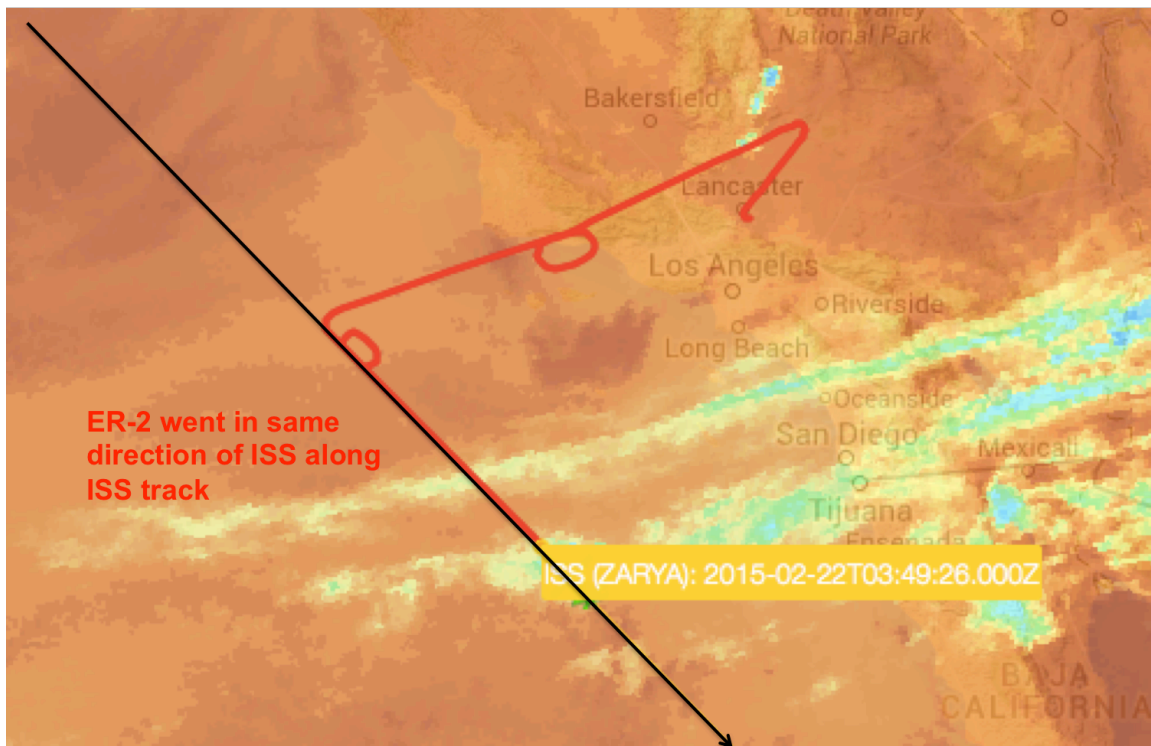


**Figure 3.2** The tracks for the ISS and NASA ER-2 near the coast of California on 22 February 2015.

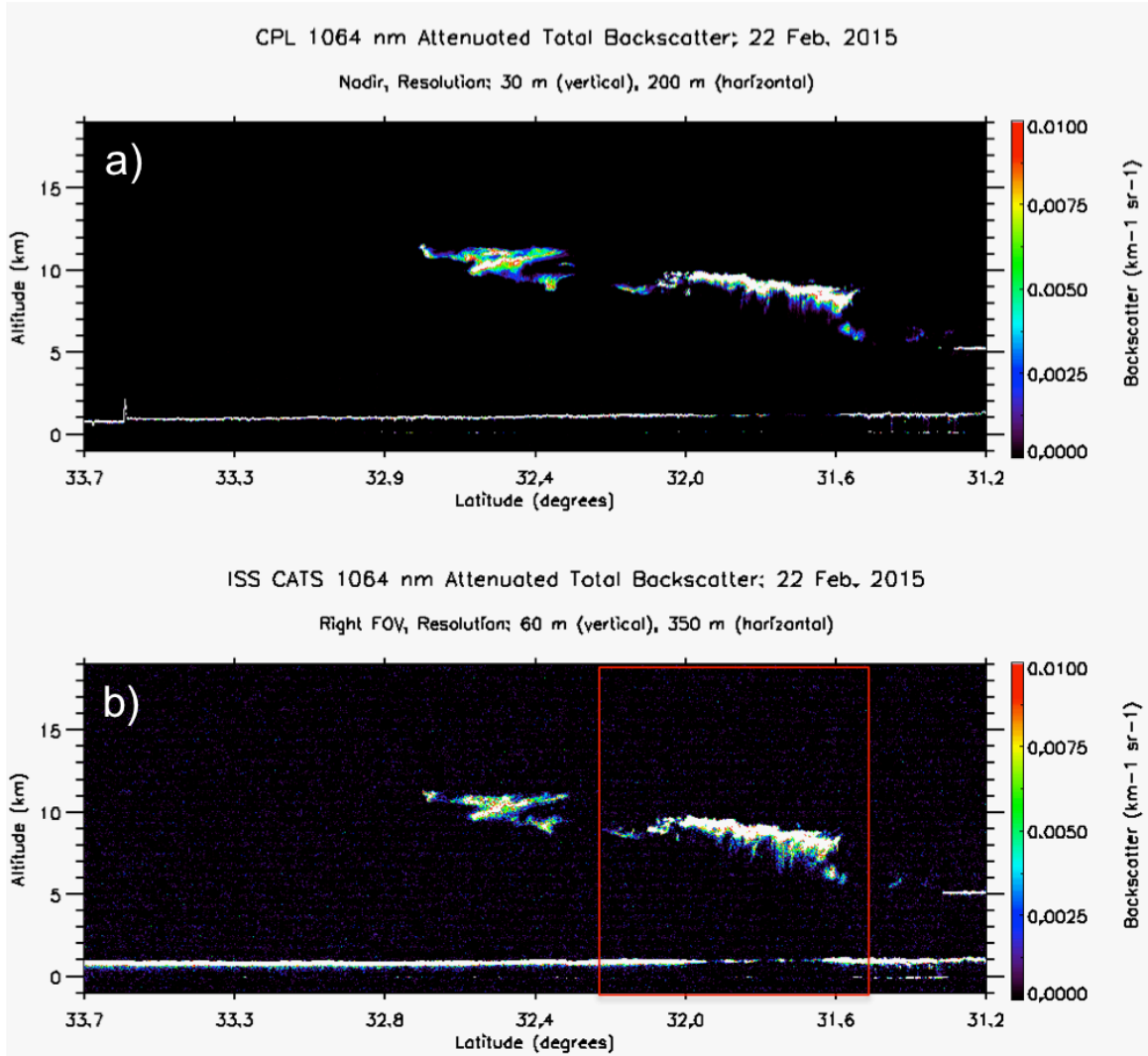
The time of closest coincidence occurs at 03:49:26 UTC near 32.0 degrees latitude as both instruments observe a dense ice cloud, as shown in the 1064 nm attenuated total backscatter data in Figure 3.3 for both CPL (a) and CATS (b). The estimate of the second PGR term relies on two assumptions:

- 1) The spectral depolarization ratio, defined as the ratio of depolarization ratio at 1064 nm to depolarization ratio at 532 nm, is unity for dense ice clouds.
- 2) The CPL 1064 nm depolarization ratios and thus attenuated perpendicular backscatter measurements are accurate to within 3%, which is the estimated crosstalk between polarization detector channels measured for the CPL instrument.

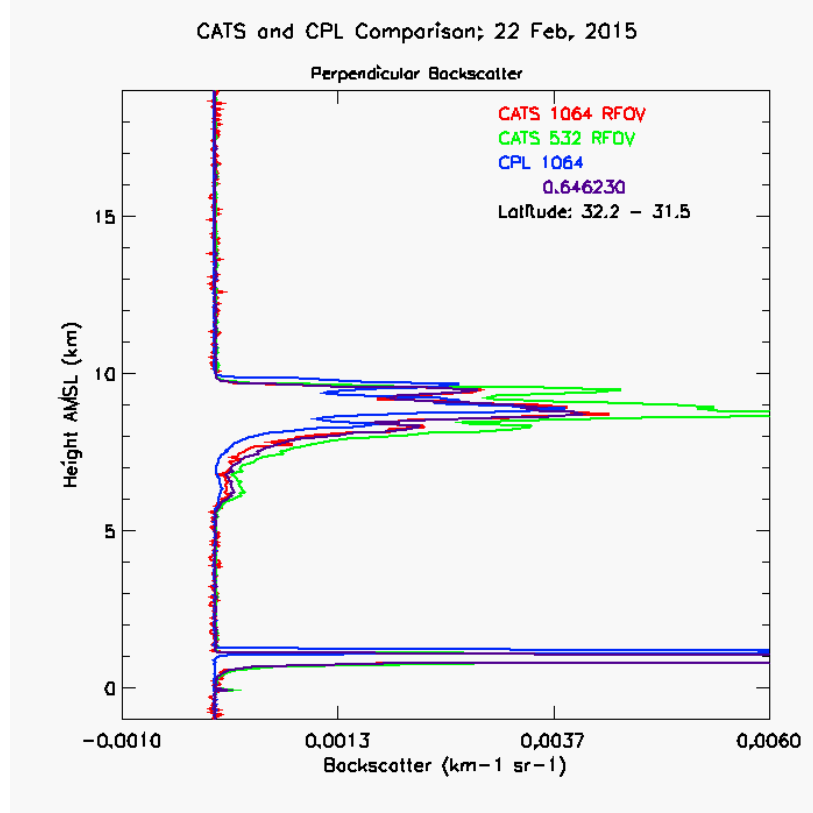
Under these two assumptions, the CPL 1064 nm attenuated perpendicular backscatter should be equivalent to the CATS attenuated perpendicular backscatter measurements at both 532 and 1064 nm for dense ice clouds.

Figure 3.4 shows the mean attenuated perpendicular backscatter data for the profiles highlighted in the red box in Figure 3.3 for CPL 1064 nm (blue) and CATS RFOV 532 nm (green) and 1064 nm (red), after the CATS data has been normalized to Rayleigh (Section 3.2.5) and the  $PGR_1$  term has been applied to the data. The CPL 1064 nm (blue) and CATS RFOV 1064 nm (red) profiles agree very well within the dense ice cloud. However, the CATS RFOV 532 nm (green) profile is higher than both the 1064 nm profiles. A ratio of about 0.646 must be applied to the CATS 532 nm perpendicular backscatter profile (purple) to obtain a spectral depolarization ratio of 1.0 for the dense ice cloud. Thus, the  $PGR_2$  term for RFOV 532 nm is 0.646. Similarly, the LFOV 532 and 1064 nm  $PGR_2$  terms are computed using this near-coincident dataset.

Errors in the CATS polarization gain ratio are based on statistics of the derived PGR terms. The  $PGR_1$  term, computed using the ratio of the parallel to perpendicular solar background radiation scattered from dense ice clouds, typically has an error of less than 10%. The error in the second PGR term is estimated to be less than 5%.



**Figure 3.3** The 1064 nm attenuated total backscatter data for both CPL (a) and CATS (b) for the segment of the ER-2 flight along the ISS track on 22 February 2015. The red box denotes the profiles averaged to create Figure 3.4.



**Figure 3.4** The mean attenuated perpendicular backscatter data for the profiles highlighted in the red box in Figure 3.3 for CPL 1064 nm (blue) and CATS RFOV 532 nm (green) and 1064 nm (red). The CATS RFOV 532 nm data multiplied by 0.646 is shown in the purple profile.

### 3.2.4 Stratospheric Scattering Ratios

The CATS calibration coefficients are computed by normalizing the normalized relative backscatter signal with respect to a modeled molecular backscatter signal over a set altitude range of 23 to 27 km. This altitude regime was selected because the CATS data frame is restricted to an upper limit of 28 km above mean sea level and tropical cirrus and volcanic plumes typically extend as high as 18 and 22 km respectively (although the latter depends on the magnitude of each volcanic eruption). Although the aerosol loading in this region is generally less than would be found in the lower stratosphere, it is not free of aerosol contamination. Thus to accurately normalize the NRB signal to the molecular backscatter model, the aerosol loading must be characterized by a spatially and temporally varying ratio of total backscatter to molecular backscatter, referred to as the scattering ratio ( $R$ ) and defined as:

$$R_{\lambda}(r) = \frac{\beta_{tot}(r)T_{tot}^2(r)}{\beta_M(r)T_M^2(r)T_{O_3}^2(r)} \quad \text{Eq. 3.21}$$

The 532 nm scattering ratios in the CATS calibration region are estimated using the CALIPSO V4 Level 1 data. Monthly HDF files are provided by the CATS LaRC team



every 15 days that include the profiles of the 30-day mean, median, standard deviation, and error of the 532 nm scattering ratio between 22 and 28 km (180 m bins) and between 54 S and 54 N degrees latitude at 2 degree latitude increments. The scattering ratio varies by latitude and altitude, with values as high as 1.22 in the lower stratosphere (22 km) near the equator as shown in Figure 3.5 for February 2007. The most recent monthly HDF file is used to derive the 532 scattering ratio in the CATS calibration algorithm and to estimate the 1064 nm scattering ratio using the equation:

$$R_{1064}(r) = 1 + \frac{\chi_{1064}(\beta_{M,532}(r)R_{532}(r) - 1)}{\beta_{M,1064}(r)} \quad \text{Eq. 3.22}$$

where  $\beta_m$  at 532 and 1064 nm are the Rayleigh backscatter model computed as shown in section 3.2.2 and  $\chi_{1064}$  is the backscatter color ratio defined as:

$$\chi_{1064} = \frac{\beta_{P,1064}(r)}{\beta_{P,532}(r)} = 0.40 \quad \text{Eq. 3.23}$$

The application of the 532 and 1064 nm scattering ratios will be discussed in the next section.

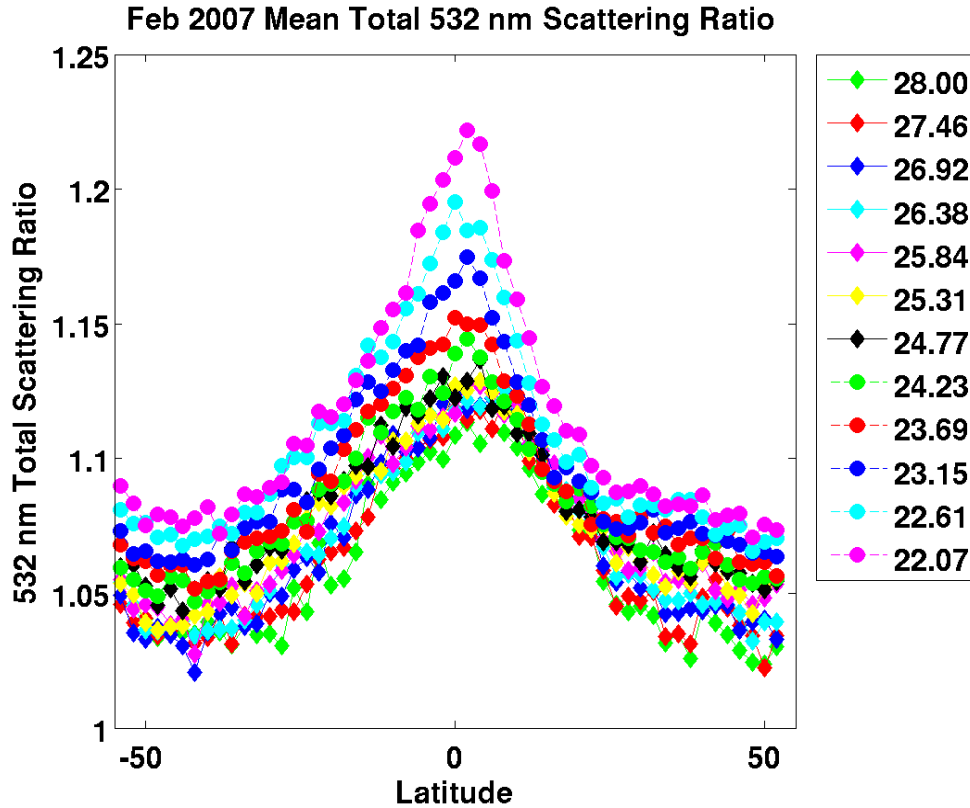


**Figure 3.5** The mean CALIPSO scattering ratios for February 2007 for various altitude bins between 22 and 28 km.

### 3.2.5 Calibration at 532 and 1064 nm Wavelengths

Once the ozone transmission, Rayleigh scattering, polarization gain ratio, and stratospheric scattering ratios have been computed, the next step in the calibration of CATS data is to apply these parameters to the CATS data. The perpendicular NRB at raw resolution is multiplied by the PGR at both the 532 and 1064 nm wavelengths. The total NRB signal at both wavelengths, derived by adding the perpendicular and parallel signals ( $\text{NRB}_{\text{perp}} + \text{NRB}_{\text{par}}$ ), is then divided by both the ozone transmission and stratospheric scattering ratio of the corresponding wavelength as a function of height. This CATS calibration-ready NRB signal is averaged to 4 minute segments at night and 46 minute segments during daytime operation to create mean profiles of the calibration-ready NRB in the calibration region of 23-27 km.

The 532 and 1064 nm CATS calibration coefficient (C) profiles at each segment are derived by normalizing the mean calibration-ready NRB signal ( $\beta_{\text{CN}}$ ) to the mean molecular backscatter signal ( $\beta_{\text{M}}T_{\text{M}}^2T_{\text{O}}^2$ ) in the calibration region (Russell *et al.* 1979, Del Guasta 1998, McGill *et al.* 2007, Powell *et al.* 2009), as shown in the equation below:

$$C_{\lambda}(r) = \frac{\bar{\beta}_{\text{CN}}(r)}{\bar{\beta}_{\text{M}}(r)\bar{T}_{\text{M}}^2(r)\bar{T}_{\text{O}_3}^2(r)} \quad \text{Eq. 3.24}$$

The final calibration coefficient at each segment (typically 4 mins for night, 46 mins for day) is simply the mean of the calibration coefficient profile from 23 to 27 km. For nighttime conditions, this provides 10-20 calibration coefficients per granule compared to only 1-2 per daytime granules. The final calibration constant is computed by either calculating the mean of the calibration coefficient data points in each granule or by a linear fit (pre-determined by Mode and SNR), as shown in Figure 3.6. If the calibration coefficient at a specific segment does not meet a threshold value, it is not used in the average or fit. In daytime granules, it is possible that no calibration coefficients meet these threshold values. When this occurs, a default calibration constant is set for the entire granule based on historical data and/or manual normalization to the modeled Rayleigh signal. It should be noted that the CATS 1064 nm calibration constant is also derived using the 532 nm signal and backscatter from ice clouds, similar to CALIPSO at 1064 nm (Vaughan *et al.* 2010), but is not used operationally. This technique is only used for research purposes by the CATS team to compare the two 1064 nm calibration techniques.

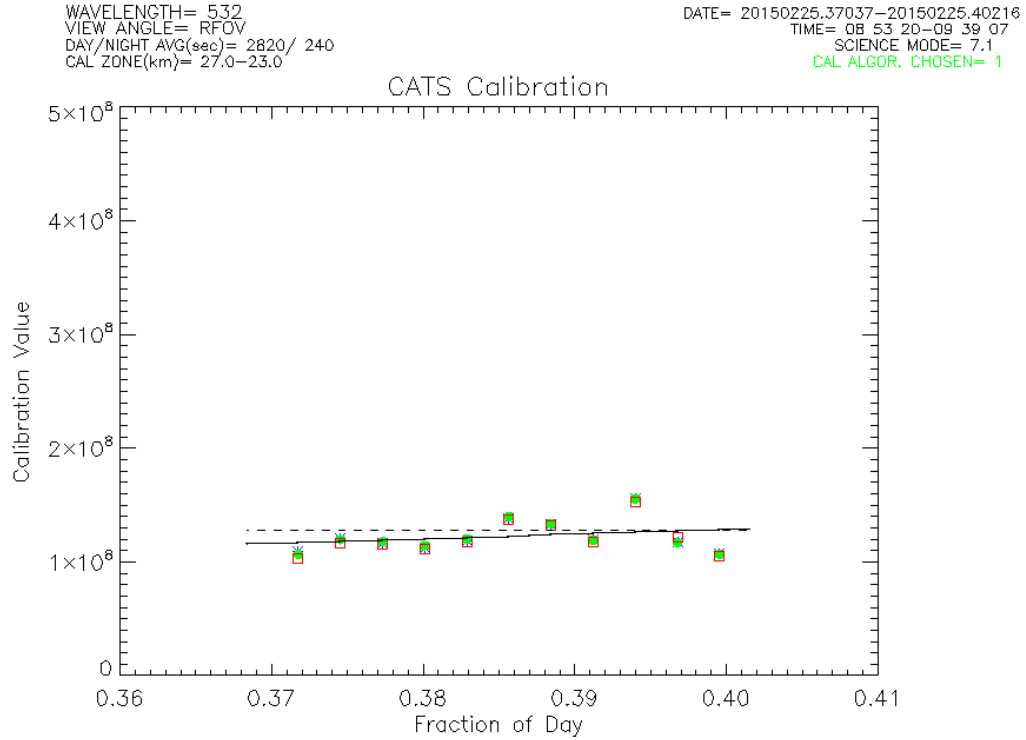


**Figure 3.6** The 532 nm RFOV calibration coefficients (green) computed during a nighttime granule on 25 Feb. 2015 around 08 UTC. The linear fit apply to the data (black solid line) is the calibration constant applied to the backscatter data. The dotted black line is the default value that would be used if the calibration coefficients were not within thresholds.

There are two main types of error in the CATS calibration constant: systematic error and random error. The systematic error in the CATS calibration constant is derived similar to the systematic error in the CALIPSO calibration (Reagan *et al.* 2002, Powell *et al.* 2009). This systematic error has four sources:

- 1) Error in the stratospheric scattering ratios provided by CALIPSO ( $\Delta R$ )
- 2) Error in the molecular backscatter coefficient derived from the GMAO data ( $\Delta \beta_M$ )
- 3) Error in the background transmission from molecules and ozone in the atmosphere ( $\Delta T^2$ )
- 4) Errors induced by non-ideal optical performance of the CATS lidar system ( $\epsilon + a + c$ ). This error can be effectively reduced by instrument corrections.

Thus the total relative systematic error in the calibration constant is defined as:

$$\left(\frac{\Delta C}{C}\right)_{sys}^2 = \left(\frac{\Delta R}{R}\right)^2 + \left(\frac{\Delta \beta_M}{\beta_M}\right)^2 + \left(\frac{\Delta T^2}{T^2}\right)^2 + (\epsilon + a + c)^2 \quad \text{Eq. 3.25}$$

and is estimated to be 5%. The latter 3 terms are constant over time, but the error in the stratospheric scattering ratio is computed for each monthly HDF file described in section 3.2.4 and varies by season and volcanic activity.

The random error in the calibration constant results from normalizing the 532 and 1064 nm signals to the modeled molecular signal and is dominated by noise in the lidar signal. This error can be estimated by determining the variability of the intermediate calculated coefficients ( $C_i$ ) computed at each averaging segment (4 minutes for nighttime data) that are averaged to produce the final calibration constants. As described above, the intermediate calibration coefficients are computed for each vertical bin inside the calibration zone after averaging horizontally to get a profile for the mean calibration segment with 66 vertical bins (60 m bin size). Thus the equation for computing the random error is:

$$(\Delta C)_{ran} = \frac{stdev(C_i)}{\sqrt{N}} \quad \text{Eq. 3.26}$$

Typical values of the random error for the CATS calibration constant are 5-7% at 532 nm and 1064 nm. Thus the total error is derived using the equation:

$$\left(\frac{\Delta C}{C}\right)_{tot}^2 = \left(\frac{\Delta C}{C}\right)_{sys}^2 + \left(\frac{\Delta C}{C}\right)_{ran}^2 \quad \text{Eq. 3.27}$$

The total error in the CATS calibration constants at 532 and 1064 nm is estimated at 5-10%.

### 3.2.6 Attenuated Backscatter

The primary product in the CATS Level 1B data is the calibrated backscatter, known as the attenuated total backscatter (ATB or  $\gamma$ ), which has units of  $\text{km}^{-1} \text{sr}^{-1}$  and is defined as:

$$\gamma(r) = \frac{NRB(r)}{C} = [\beta_P(r) + \beta_M(r)]T_M^2(r)T_P^2(r) \quad \text{Eq. 3.28}$$

Where  $C$  is the calibration constant determined using the algorithm outlined in section 3.2.5. The attenuated backscatter is also computed for the perpendicular and parallel signals using the same calibration constant as the total signal. The primary sources of uncertainty in the CATS attenuated backscatter signal are the calibration constant and signal noise. Thus if the calibration constant is accurate, the CATS ATB profiles should compare favorably with the Rayleigh backscatter model, as shown in Figure 3.7.

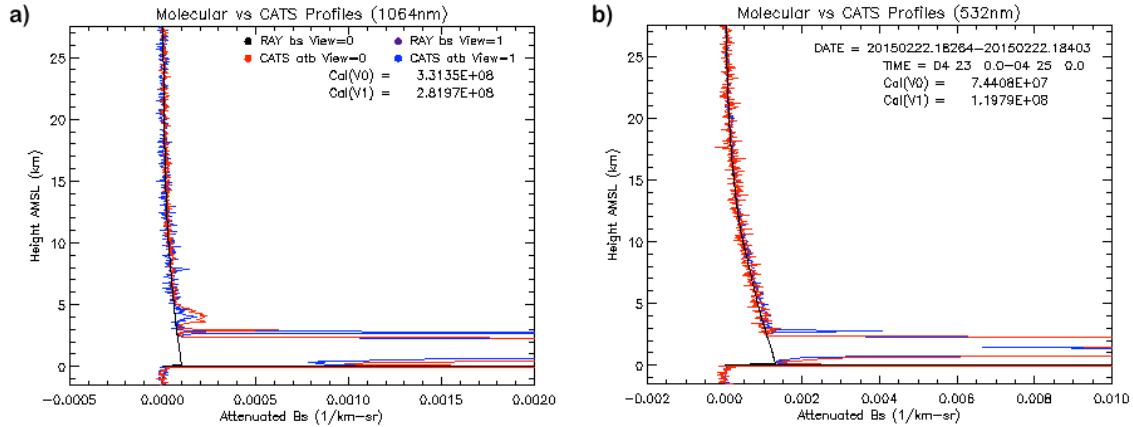


**Figure 3.7** The 2-minute mean profiles of the CATS ATB signal at 1064 (a) and 532 (b) for both the RFOV (red) and LFOV (blue) for data on 22 February 2015. These profiles compared favorably with the modeled Rayleigh profiles (black) for each wavelength and field-of-view, demonstrating that the data is well calibrated.

## 4.0 Overview of Vertical Feature Mask Algorithms

There will be two CATS Level 2 products and therefore two vertical feature mask algorithms. The CATS Heritage Level 2 products (Rodier *et al.* 2015) are created when CATS L1B files are run through the CALIPSO L2 algorithms to provide continuity in the algorithms used for the lidar climate record. These algorithms are outlined in detail in the CALIPSO ATBD (Vaughan *et al.* 2005) and in numerous publications (Hu *et al.* 2009, Liu *et al.* 2009, Omar *et al.* 2009, Vaughan *et al.* 2009, Young *et al.* 2009), so they will not be discussed in this document. The CATS Operational L2 products are produced using new operational CATS L2 algorithms, which will include new capabilities that correspond to new instrument technology such as spectral depolarization and high resolution 1064 nm data. These CATS Operational vertical feature mask algorithms will be outlined in the sections to follow in future releases.

### 4.1 Atmospheric Layer Detection

Details to come in future versions.

### 4.2 Cloud-Aerosol Discrimination

Details to come in future versions.

### 4.3 Cloud Phase

Details to come in future versions.

### 4.4 Aerosol Typing

Details to come in future versions.

## **5.0 Overview of Geophysical Parameter Algorithms**

Details to come in future versions.

### **5.1 Parameterized Lidar Ratio**

Details to come in future versions.

### **5.2 Constrained Lidar Ratio**

Details to come in future versions.

### **5.3 Modified Lidar Ratio**

Details to come in future versions.

## **References**

- Behrendt, A.; T. Nakamura, 2002: Calculation of the calibration constant of polarization lidar and its dependency on atmospheric temperature. *Optics Express*, Vol. 10, No. 16, p. 805-817.
- Bodhaine B. A., N. B. Wood, E. G. Dutton, and J. R. Slusser, 1999: On Rayleigh optical depth calculations. *J. Atmos. Ocean Technol.*, 16, 1854-1861.
- Bucholtz, A., 1995: Rayleigh-scattering calculations for the terrestrial atmosphere. *Appl. Opt.*, 34, 2765-2773.
- Collis, R. T. H., and P. B. Russell, 1976: Lidar measurement of particles and gases by elastic backscattering and differential absorption”, *Laser Monitoring of the Atmosphere*, E. D. Hinkley (editor), (Springer-Verlag, 1976), Chapter 4.
- Del Guasta, M., 1998: Errors in the retrieval of thin-cloud optical parameters obtained with a two-boundary algorithm, *Appl. Opt.*, 37, 5522–5540.
- Fernald, F.G., B. M. Herman and J. A. Reagan, 1972: “Determination of aerosol height distributions with lidar”, *Journal of Applied Meteorology*, **11**, 482-489.
- Hlavka, D. L., J. E. Yorks, S. A. Young, M. A. Vaughan, R. E. Kuehn, M. J. McGill, and

- S. D. Rodier, 2012: Airborne validation of cirrus cloud properties derived from CALIPSO lidar measurements: Optical properties. *J. Geophys. Res.*, **117**, D09207, doi:10.1029/2011JD017053.
- Hovis, F.E. , M. Rhoades, R. L. Burnham, J. D. Force, T. Schum, B. M. Gentry, H. Chen, S. X. Li, J. W. Hair, A. L. Cook, and C. A. Hostetler, 2004: Single-frequency lasers for remote sensing. *Proc. SPIE* 5332, 263–270.
- Hu, Y., Z. Liu, D. Winker, M. Vaughan, V. Noel, L. Bissonnette, G. Roy, and M. McGill, 2006: A simple relation between lidar multiple scattering and depolarization for water clouds. *Optics Letters*, **31**, 1809-1811.
- Hu, Y., and coauthors, 2009: CALIPSO/CALIOP cloud phase discrimination algorithm, *J. Atmos. Oceanic Technol.*, **26**, 2293–2309. doi:10.1175/2009JTECHA1280.1.
- Iqbal, M., 1983: *An Introduction to Solar Radiation*, Academic Press, New York, NY.
- Klett, J. D., 1981: Stable analytical inversion solution for processing lidar returns. *Appl. Opt.*, **20**, 211–220.
- Klett, J. D., 1985: Lidar inversion with variable backscatter/extinction ratios. *Appl. Opt.*, **24**, 1638–1643.
- Liou, K. N., Y. Takano, and P. Yang *et al.*, 2000: Light scattering and radiative transfer in ice crystal clouds: applications to climate research. in *Light Scattering by Nonspherical Particles*, M. Mishchenko *et al.*, Eds. San Diego, CA: Academic, pp. 417–449.
- Liu, Z., M. McGill, Y. Hu, C.A. Hostetler, M. Vaughan, and D. Winker, 2004: Validating lidar depolarization calibration using solar radiation scattered by ice clouds. *Geoscience Remote Sensing Letters*, **1**, doi: 10.1109/LGRS.2004.829613.
- Liu, Zhaoyan, and coauthors, 2009: The CALIPSO Lidar Cloud and Aerosol Discrimination: Version 2 Algorithm and Initial Assessment of Performance, *J. Atmos. Oceanic Technol.*, **26**, 1198–1213.
- McGill, M. J., M. Marzouk, V. S. Scott, and J. D. Spinhirne, 1997c: Holographic circle-to-point converter with particular applications for lidar work, *Opt. Eng.*, **36**, 2171–2175.
- McGill, M.J., and R.D. Rallison, 2001: Holographic optics convert rings to points for Detection. *Laser Focus World*, **37**, 131-136.
- McGill, M. J., D. Hlavka, W. Hart, V. S. Scott, J. Spinhirne, and B. Schmid, 2002: Cloud Physics Lidar: instrument description and initial measurement results. *Applied Optics*, **41**, 3725-3734.

- McGill, M.J., D.L. Hlavka, W.D. Hart, E.J. Welton, and J.R. Campbell, 2003: Airborne lidar measurements of aerosol optical properties during SAFARI-2000. *Journal of Geophysical Research*, 108, doi: 10.1029/2002JD002370.
- McGill, M. J., M. A. Vaughan, C. R. Trepte, W. D. Hart, D. L. Hlavka, D. M. Winker, and R. Kuehn, 2007: Airborne validation of spatial properties measured by the CALIPSO lidar. *J. Geophys. Res.*, **112**, D20201, doi:10.1029/2007JD008768.
- Omar, Ali H., and coauthors, 2009: The CALIPSO Automated Aerosol Classification and Lidar Ratio Selection Algorithm, *J. Atmos. Oceanic Technol.*, 26, 1994–2014.
- Palm, S., W. Hart, D. Hlavka, E. J. Welton, A. Mahesh, and J. Spinhirne, 2002: GLAS atmospheric data products. NASA Goddard Space Flight Center Geoscience Laser Altimeter System Algorithm Theoretical Basis Document Version 4.2, 141 pp.
- Powell, Kathleen A., and coauthors, 2009: CALIPSO Lidar Calibration Algorithms. Part I: Nighttime 532-nm Parallel Channel and 532-nm Perpendicular Channel, *J. Atmos. Oceanic Technol.*, 26, 2015–2033.
- Privé, N. C., R. M. Errico, and K-S. Tai, 2013: Validation of the forecast skill of the Global Modeling and Assimilation Office observing system simulation experiment. *Quarterly Journal of the Royal Meteorological Society* 139.674, 1354-1363.
- Rienecker, M. M. et al, 2008: The GEOS-5 Data Assimilation System—Documentation of Versions 5.0. 1, 5.1. 0, and 5.2. 0. NASA Tech. Memo104606.27 (2008).
- Rodier, S., M. Vaughan, S. Palm, J. Yorks, M. McGill, M. Jensen, T. Murray, K.-P. Lee and C. Trepte, 2015: Laser Remote Sensing from ISS: CATS Cloud and Aerosol Data Products, proceedings of the ILRC 2015, New York, New York.
- Rogers, R. R., Hair, J. W., Hostetler, C. A., Ferrare, R. A., Obland, M. D., Cook, A. L., Harper, D. B., Burton, S. P., Shinozuka, Y., McNaughton, C. S., Clarke, A. D., Redemann, J., Russell, P. B., Livingston, J. M., and Kleinman, L. I., 2009: NASA LaRC airborne high spectral resolution lidar aerosol measurements during MILAGRO: observations and validation. *Atmos. Chem. Phys.*, 9, 4811-4826, doi:10.5194/acp-9-4811-2009.
- Russell, P. B., T. J. Swissler, and M. P. McCormick, 1979: Methodology for error analysis and simulation of lidar aerosol measurements, *Appl. Opt.*, 18, 3783–3797.
- Sassen, K., and S. Benson, 2001: A midlatitude cirrus cloud climatology from the Facility for Atmospheric Remote Sensing. Part II: Microphysical properties derived from lidar depolarization. *J. Atmos. Sci.*, 58, 2103– 2112.



- Sassen, K., 2002: Cirrus: A modern perspective. *Cirrus*, D. K. Lynch *et al.*, Eds., Oxford University Press, 11–40.
- She, C., 2001: Spectral structure of laser light scattering revisited: bandwidths of nonresonant scattering lidars”, *Appl. Opt.*, 40, 4875-4884.
- Spinhirne J. D., J. A. Reagan, and B. M. Herman, 1980: Vertical distribution of aerosol extinction cross section and inference of aerosol imaginary index in the troposphere by lidar technique. *J. Appl. Meteor.*, **19**, 426–438.
- Spinhirne, J. D., M. Z. Hansen, and L. O. Caudill, 1982: Cloud top remote sensing by airborne lidar. *Appl. Opt.*, vol. 21, pp. 1564–1571.
- Tenti, G., C. D. Boley, and R. C. Desai, 1974: On the kinetic model description of Rayleigh–Brillouin scattering from molecular gases. *Can. J. Phys.*, **52**, 285–290.
- Vaughan, M. A., and coauthors, 2004: Fully automated analysis of space –based lidar data: An overview of the CALIPSO retrieval algorithms and data products, *Proc. SPIE*, 5575, 16-30.
- Vaughan, M. A., D. M. Winker, and K. A. Powell, 2005: Part 2: Feature Detection and Layer Properties Algorithms. CALIOP Algorithm Theoretical Basis Document PC-SCI-202.01, 87 pp.
- Vaughan, M., and coauthors, 2009: Fully automated detection of cloud and aerosol layers in the CALIPSO lidar measurements, *J. Atmos. Oceanic Technol.*, 26, 2034–2050.
- Vaughan, M. A., Z. Liu, M. J. McGill, Y. Hu, and M. D. Obland, 2010: On the spectral dependence of Backscatter from cirrus clouds: Assessing CALIOP’s 1064 nm calibration assumptions using cloud physics lidar measurements, *J. Geophys. Res.*, 115, D14206, doi:10.1029/2009JD013086.
- Vermeille, H., 2002: Direct Transformation from geocentric coordinates to geodetic coordinates. *Journal of Geodesy*, 76:451-454.
- Vigroux, E., 1953: Contribution a l'etude experimentale de l'absorption de l'ozone, *Ann. Phys.*, 8, 709-761.
- Winker, D. M., 2003: Accounting for multiple scattering in retrievals from space lidar. *Lidar Scattering Experiments*, C. Werner, U. Oppel, and T. Rother, ed., International Society for Optical Engineering (SPIE Proceedings, Vol. 5059), 128–139.
- Winker, D. M., M. A. Vaughan, A. H. Omar, Y. Hu, K. A. Powell, Z. Liu, W. H. Hunt,

- and S. A. Young, 2009: Overview of the CALIPSO Mission and CALIOP Data Processing Algorithms. *J. Atmos. Oceanic Technol.*, **26**, 1105–1119, doi:10.1175/2009JTECHA1281.1.
- Yorks, J. E., D. L. Hlavka, W. D. Hart, M. J. McGill, 2011a: Statistics of Cloud Optical Properties from Airborne Lidar Measurements. *J. Atmos. Oceanic Technol.*, **28**, 869–883. doi: <http://dx.doi.org/10.1175/2011JTECHA1507.1>
- Yorks, J. E., D. L. Hlavka, M. A. Vaughan, M. J. McGill, W. D. Hart, S. Rodier, and R. Kuehn, 2011b: Airborne validation of cirrus cloud properties derived from CALIPSO lidar measurements: Spatial properties, *J. Geophys. Res.*, **116**, D19207, doi:10.1029/2011JD015942.
- Yorks, J. E., M. McGill, V. S. Scott, A. Kupchock, S. Wake, D. Hlavka, W. Hart, P. Selmer, 2014a: The Airborne Cloud-Aerosol Transport System: Overview and Description of the Instrument and Retrieval Algorithms, *J. Atmos. Oceanic Technol.*, **31**, 2482–2497, doi:10.1175/JTECH-D-14-00044.1.
- Young, A.T., 1981: Rayleigh scattering. *Phys. Today*, **35**, 42–48.
- Young, S. A., 1995: Analysis of lidar backscatter profiles in optically thin clouds, *Appl. Opt.*, **34**, 7019–7031.
- Young, S. A., and M. A. Vaughan, 2009: The retrieval of profiles of particulate extinction from Cloud-Aerosol Lidar Infrared Pathfinder Satellite Observations (CALIPSO) data: Algorithm description. *J. Atmos. Oceanic Technol.*, **26**, 1105–1119.
- Young, Stuart A., Mark A. Vaughan, Ralph E. Kuehn, David M. Winker, 2013: The Retrieval of Profiles of Particulate Extinction from Cloud–Aerosol Lidar and Infrared Pathfinder Satellite Observations (CALIPSO) Data: Uncertainty and Error Sensitivity Analyses. *J. Atmos. Oceanic Technol.*, **30**, 395–428. doi: <http://dx.doi.org/10.1175/JTECH-D-12-00046.1>